

Velocity selection of ultra-cold atoms with Fabry-Perot laser devices: improvements and limits

A. Ruschhaupt, F. Delgado, and J. G. Muga
Departamento de Química-Física, UPV-EHU,
Apartado 644, 48080 Bilbao, Spain

We discuss a method to select the velocities of ultra-cold atoms with a modified Fabry-Perot type of device made of two effective barriers and a well created, respectively, by blue and red detuned lasers. The laser parameters may be used to select the peak and width of the transmitted velocity window. In particular, lowering the central well provides a peak arbitrarily close to zero velocity having a minimum but finite width. The low-energy atomic scattering off this laser device is parameterized and approximate formulae are found to describe and explain its behaviour.

PACS numbers: 32.80.Pj, 42.50.Vk, 03.75.-b

Velocity selection is a basic operation in quantum optics and atomic physics for a plethora of applications. There are mechanical (slotted disks) and non-mechanical (optical) techniques available, useful for different experimental circumstances, species, and energies. The large wavelengths achieved with laser cooling have made the traditional methods no longer effective because of the increasing importance of gravity and the quantum nature of translational motion. For example, the standard classical-mechanical analysis of mechanical velocity-selection methods becomes invalid for small-time temporal slits, since they produce momentum spread in agreement with a time-energy uncertainty principle [1]. Among the new methods, the velocity selection using Doppler sensitive stimulated Raman transitions [2], and coherent population trapping into a dark state [3], provide selectivity in the “transverse direction” parallel to the lasers, and rely on specific internal level configurations. Fabry-Perot (FP) cavities have been also proposed to provide coherent velocity selection or trapping for longitudinal motion, using detuned lasers perpendicular to the incident atoms [4] or microwave cavities [5, 6] to implement the partially reflecting mirrors. The velocity selection in these cavities is produced by the filtering effect of resonance peaks in the transmission probability. The potential of FP cavities as trapping devices also stems from characteristic resonance features: high densities and large life times in the interaction region.

The aim of this work is to discuss an improvement of these cavities, provide formulae to describe their be-

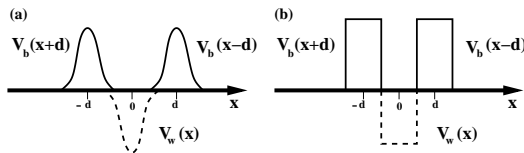


FIG. 1: $m = \text{mass}(^{23}\text{Na})$; (a) Gaussian functions, $d = 6 \mu\text{m}$, $\sigma = 2 \mu\text{m}$; (b) square functions, $d = 5 \mu\text{m}$

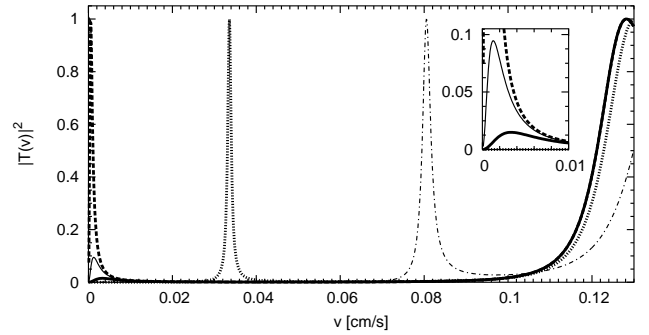


FIG. 2: Transmittance versus velocity for different well depths. $\widehat{V}_b = 300 \hbar/s$; $\widehat{V}_w = 0$ (dashed-dotted line), $\widehat{V}_w = 150 \hbar/s$ (thick dotted line), $\widehat{V}_w = 180.2 \hbar/s$ (thick dashed line), $\widehat{V}_w = 180.25 \hbar/s$ (solid line), $\widehat{V}_w = 180.5 \hbar/s$ (thick solid line); other parameters in Fig. 1a. The inset is a zoom of the lower-left corner.

haviour, and study the fundamental limitations to lower the peak width and velocity of the transmitted wave packet. The basic idea is to add a well with controllable depth between the two external barriers, see Fig. 1. Effective barriers and well can be implemented with blue and red detuned lasers, respectively, which do not excite the impinging ground state atom and cause only a mechanical effect. The depth of the well and the barrier height can be varied with the intensities of the lasers. Making the well deeper, rather than wider, displaces the resonance peaks to lower energies without diminishing the inter-resonance spacing so it is the ideal way to achieve a sharp low-energy velocity selection. The resonance peak displacement with the well-depth can be seen in Fig. 2. The velocity shift is accompanied by a peak width reduction until a minimum, non-zero width is attained when the peak reaches zero velocity at a critical “threshold” depth. Beyond that depth the peak broadens, moves to higher velocities, and its maximum decays, as shown in the inset of Fig. 2. The effects of different depths are summarized in Fig. 3, which will be explained

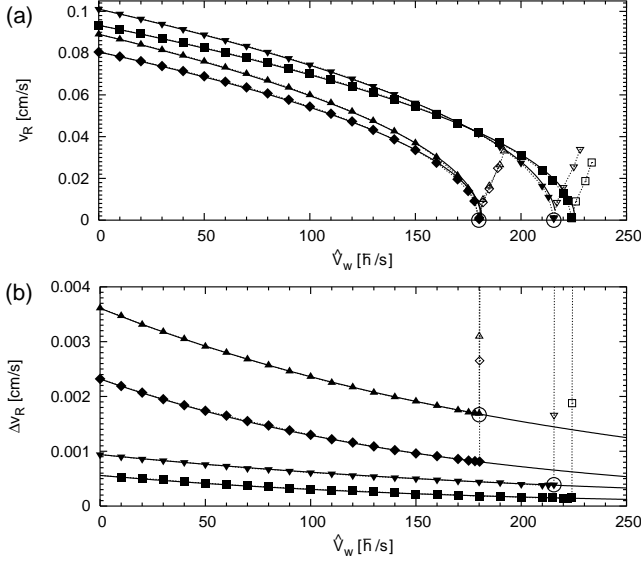


FIG. 3: (a) Resonance velocity v_R versus \hat{V}_w (symbols connected with dotted line). Filled symbols indicate the case $|T(v_R)|^2 > 0.995$, and empty symbols otherwise. The solid lines show the approximation of Eq. (4). Gaussian functions, see Fig. 1a: $\hat{V}_b = 300\hbar/s$, $\alpha = 0.65$ (diamonds), $\hat{V}_b = 500\hbar/s$, $\alpha = 0.70$ (squares); square functions, see Fig. 1b: $\hat{V}_b = 300\hbar/s$, $\alpha = 0.79$ (triangles up), $\hat{V}_b = 500\hbar/s$, $\alpha = 0.85$ (triangles down), the circles indicate $\hat{V}_{w,thres}$ for the square model in the 2-pole approximation. (b) Velocity width Δv_R of the resonance versus \hat{V}_w ; meaning of symbols as in (a). The solid lines show the approximation of Eq. (5), the circles indicate $(\hat{V}_{w,thres}, \Delta v_{R,thres})$ with the 2-pole approximation.

next in more detail.

We shall use both a realistic model based on three Gaussians, see Fig. 1, as well as a simplified version with two square barriers and a well. The scattering off the two potential models is very similar but the later enables us to obtain analytical exact results and approximate but physically illuminating expressions. Let us consider, for a single ultra-cold atom, the Hamiltonian

$$H = -\frac{\hbar^2}{2m} \frac{\partial^2}{\partial x^2} + V_b(x+d) - V_w(x) + V_b(x-d), \quad (1)$$

where $V_{b,w}(x) = \hat{V}_{b,w} \Pi(x)$, and Π can take the forms

$$\Pi_G = \exp\left(-\frac{x^2}{2\sigma^2}\right), \quad \Pi_s = \begin{cases} 1 & \text{if } -d/2 < x < d/2 \\ 0 & \text{otherwise} \end{cases}$$

for the Gaussian and square models respectively. For simplicity we have set all Gaussians with the same width σ , and the square segments with the same length d . We assume that the atom impinges from the left and only initial positive velocities are considered. We are interested in the transmission amplitude T and the “transmittance” $|T|^2$ of the scattering solutions of $H\phi_v(x) = E_v\phi_v(x)$,

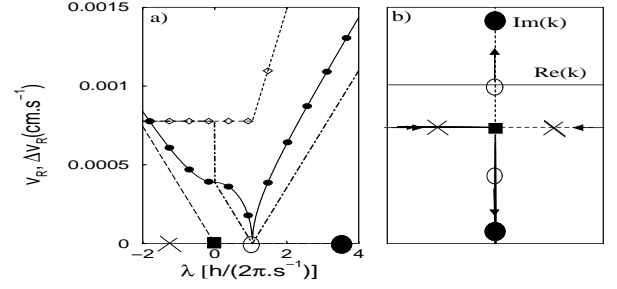


FIG. 4: Connection between peaks and poles in the square model, $\hat{V}_b = 400\hbar/s$, other parameters in Fig. 1b; for the plotted parameter range, the 2-pole approximation and the exact result are indistinguishable; (a) resonance velocity v_R (line with filled dots), resonance width Δv_R (line with unfilled diamonds) versus the distance $\pm\lambda$ of the pole to the collision ($\lambda < 0$ before the collision, $\lambda > 0$ after the collision); a 1-pole approximation with only k_1 is also plotted (v_R (dashed line), Δv_R (dashed-dotted line)). (b) Motion of the two poles: $\hat{V}_w = 199.884\hbar/s$ (crosses), $\hat{V}_{w,coll} = 199.898\hbar/s$ (coinciding squares), $\hat{V}_{w,thres} = 199.901\hbar/s$ (small circles), $\hat{V}_w = 199.92\hbar/s$ (big circles).

where $E_v = \frac{mv^2}{2} = \hbar^2 k^2 / (2m)$. Both velocity, v , and wavenumber, k , will be used, the later being more appropriate for complex plane analysis and the former for presenting the physical results. For the square model,

$$T(k) = -4e^{-2idk} k k_b^2 k_w \quad (2) \\ \times \left\{ e^{id(k-k_w)} [ik_b(k+k_w)C + (kk_w - k_b^2)S]^2 \right. \\ \left. - e^{id(k+k_w)} [-ik_b(k-k_w)C + (kk_w + k_b^2)S]^2 \right\}^{-1}$$

where $C = \cosh(dk_b)$, $S = \sinh(dk_b)$, $k_w = (k^2 + K_w^2)^{1/2}$, $k_b = (K_b^2 - k^2)^{1/2}$, and $K_b = (2m\hat{V}_b)^{1/2}/\hbar$, $K_w = (2m\hat{V}_w)^{1/2}/\hbar$.

In both models, at some critical, “threshold” well-depths $\hat{V}_{w,thres}$ new bound states are formed, and for well-depths close to these thresholds, the description of the transmission peak is not as simple as for isolated Breit-Wigner (BW) resonances (see Fig. 4). At a depth $\hat{V}_{w,coll}$ slightly before threshold, a resonance-antiresonance pole collision occurs, and with further deepening, two “virtual” states in the complex momentum plane appear. Centering our attention on the first, lowest-energy resonance at zero well-depth, one can distinguish when increasing the well-depth: first an ordinary resonance regime with a BW transmittance peak; second, an intermediate pre-bound state regime near threshold, in which the second pole cannot be ignored; and finally a bound-state regime. In Figure 2 transmittance curves corresponding to the different regimes are depicted. Even though the calculations can be made exactly, it is useful for applications and physically illuminating to describe these three stages in terms of approximate expressions and dominant dependences relating: poles of T in the

complex momentum plane; well-depth or other potential parameters; and visible features such as position and width of the resonance.

The first stage, dominated by a BW resonance pole k_1 in the fourth quadrant of the momentum complex plane, is the most important one for velocity selection since it allows to diminish the resonance velocity and width by deepening the well, see Figs. 2 and 3a. k_1 is accompanied by an antiresonance at $k_2 = -k_1^*$. Since the barrier is symmetrical with respect to parity, the (Gamow) resonance states have well defined parity. Thus they appear alternatively in one of the two eigenvalues of the 2×2 S matrix, for symmetrical, S_0 , or antisymmetrical scattering, S_1 . The transmission amplitude is given by $T = (S_0 + S_1)/2$. We shall follow the motion of the first symmetrical resonance, the one that will become the ground state for deep enough wells, and assume that the first antisymmetrical pole of S_1 is far from the origin so that a two pole approximation suffices. Retaining only two poles in the canonical pole expansion for cut-off potentials,

$$S_0 = -e^{-2ikr} \frac{(k - k_1^*)(k - k_2^*)}{(k - k_1)(k - k_2)}, \quad S_1 = e^{-2ikr}. \quad (3)$$

Here r is $3d/2$ for the square model. For the Gaussian model, we could truncate the potential at a large r value and apply Eq. (3). In any case the phase factor does not play any role to calculate the filtering function $|T|^2$.

Expressions for the two important poles can be obtained with the square model under some approximations, as we shall see later on. In the ‘‘BW’’ regime the antiresonance k_2 may normally be ignored if the resonance is sharp (i.e. k_1 is close to the real axis) and far from the origin. A decrease in the well-depth displaces k_1 to the left and upwards, so that the transmittance curve decreases both its peak velocity and width. By inspection of the S matrix, it is clear that in this regime the transmittance reaches the unitary limit $|T|^2 = 1$ close to $\Re(k_1)$. We define $E_R = mv_R^2/2$ and v_R as the energy and velocity of the transmittance maximum. In the BW regime $E_R \approx \hbar^2 \Re(k_1)^2/2m$. Simple parameterizations of this regime are provided by perturbation or semiclassical formulae. Let E_{R0} and v_{R0} be the real energy and velocity of the resonance peak ‘‘without well’’ ($\widehat{V}_w = 0$). Then the energy of the resonance with non-zero well can be approximated within a perturbation theory for resonance functions [7]. Up to first order in \widehat{V}_w ,

$$E_R = E_{R0} - \alpha \widehat{V}_w, \quad v_R = \sqrt{v_{R0}^2 - 2\alpha \widehat{V}_w/m}. \quad (4)$$

A semiclassical treatment [8] for opaque barriers gives $\alpha = 1$, but keeping α as a fitting parameter the dependence of Eq. (4) is valid even beyond very opaque barriers or very small depths, as can be seen in Fig. 3a. We define a velocity width Δv_R as the width of the transmittance

peak at half height. In Fig. 3b the BW regime corresponds to the slow decrease with well-depth up to the abrupt, almost vertical increase associated with a bound state. A semiclassical estimate for the energy-width of the resonance is given by a well-frequency factor times the WKB probability to escape through a barrier from the well (see e.g. [8]). Retaining dominant dependences in the opaque and shallow well limit,

$$\Delta v_R = \Delta v_{R0} \exp(-\beta \widehat{V}_w), \quad (5)$$

which, again, by keeping β as an effective fitting parameter, describes the correct behaviour in the whole BW regime, until well-depths very near the intermediate threshold region, see Fig. 3b.

Near the threshold depth the velocity and width of the peak are affected more and more by the nearby antiresonance, $k_2 = -k_1^*$. This intermediate regime is extremely narrow, with respect to variations of \widehat{V}_w , compared to the BW and bound state ones (see Fig. 4). Nevertheless, its analysis is worthwhile since it establishes the ultimate physical lower limit of the peak velocity and width using a FP filtering device. At a critical ‘‘collision’’ depth $\widehat{V}_{w,coll}$ both poles meet at $-i\kappa_{coll}$, $\kappa_{coll} > 0$, on the negative imaginary axis (see e.g. the ‘‘square’’ in Fig. 4; in one dimensional scattering, as for s-wave scattering, the collision is not at the origin because bound states are not degenerate). Note that, in spite of their zero real part, the velocity peak is not at $v = 0$. As the well becomes more profound the two poles move in opposite directions, now along the imaginary axis as ‘‘virtual’’ poles until the upper one arrives at the origin at the threshold depth $\widehat{V}_{w,thres}$, with the lower pole at $-i\kappa_{thres}$ (see e.g. ‘‘circles’’ in Fig. 4). The motion of the two poles just before the collision and even beyond threshold is well described by expanding the denominator of S_0 in powers of $(\widehat{V}_w - \widehat{V}_{w,coll})$ and retaining the first term. This gives $k_{1,2} = -i\kappa_{coll} \pm i\gamma(\widehat{V}_w - \widehat{V}_{w,coll})^{1/2}$, with γ real. A consequence is that, at threshold, $k_1 = 0$, $k_2 = -i\kappa_{thres} \approx -2i\kappa_{coll}$. The threshold is a singular, abnormal point in which the transmission peak reaches the origin, $T(0) = 1$ ($T(0) = 0$ for any other well-depth). Moreover, from the 2-pole approximation of S , $|T|^2 = \kappa_{thres}^2/(k^2 + \kappa_{thres}^2)$. Thus, the width at half height, considering only positive momenta, reaches its minimum value. In wavenumber units it is just κ_{thres} , and the maximum, $|T|^2 = 1$, occurs at $k = \kappa_{thres}$. Approximate expressions for κ_{thres} may be obtained from Eq. (2). We have to find zeros of the denominator of T . Let $\chi \equiv \frac{k}{K_b}$. We assume $\widehat{V}_b, \widehat{V}_w > 0$ and $\chi \ll 1$. Neglecting $\mathcal{O}(\chi^3)$ we arrive at the quadratic equation $\alpha_2 \chi^2 + 2i\alpha_1 \chi - \alpha_0 = 0$ with $\alpha_0 = \cot(\frac{d}{2}K_w) - K_w \coth(dK_b)/K_b$, $\alpha_1 = K_w/(2K_b \sinh^2(dK_b))$, and

$$\alpha_2 = \frac{K_b^2 (dK_w + \sin(dK_w))}{4K_w^2 \sin^2(dK_w/2)}$$

$$+ \frac{K_w (\coth(dK_b) (\cosh^2(dK_b) - 3) + dK_b)}{2K_b \sinh^2(dK_b)},$$

The two solutions are given by $\chi_{1/2} = -i\alpha_1/\alpha_2 \pm \sqrt{\alpha_0\alpha_2 - \alpha_1^2}/\alpha_2$. At $\hat{V}_{w,thres} \equiv \hbar^2 K_{w,thres}^2/2m$, a zero of the denominator of T is at $k = 0$, so $\alpha_0 = 0$. Note that if $K_b \gg 1$, $K_{w,thres} \approx \pi/d$. The other pole is at $-i\kappa_{thres} = -2iK_b\alpha_1/\alpha_2$ and determines the minimal velocity width $\Delta v_{R,thres} = \hbar\kappa_{thres}/m$ (see Fig. 3).

Finally, with further well deepening, the upper pole crosses the real axis and becomes a bound state. As predicted by Eq. (3), the transmittance peak broadens dramatically and moves to higher positive velocities; also the peak maximum becomes smaller than one, so this regime is no longer useful for velocity filtering, see Figs. 2 and 3.

As an application example we shall compute the transmitted velocity distributions resulting from the FP filtering of an atomic wavepacket prepared as a Bose-Einstein condensate [9, 10] in a trap. The trap is moved with a certain velocity with respect to the laboratory frame and turned off suddenly at $t = 0$. The condensate expands until the nonlinear interaction between the atoms can be neglected and encounters the FP cavity. (Alternatively the triple potential can be moved with the trap at rest.) First we calculate numerically the ground state $\bar{\psi}_0$ (normalized to 1) in the reference frame where the trap is at rest. A harmonic trap is assumed with frequency ω_x in x direction and ω_{yz} in y and z directions. Using a one-dimensional approximation of the Gross-Pitaevskii equation the Hamiltonian is $H(\bar{\psi}) = \frac{-\hbar^2}{2m} \frac{\partial^2}{\partial x^2} + \frac{m\omega_x^2}{2} x^2 + 2\hbar N a \omega_{yz} |\bar{\psi}(x)|^2$, where N is the number of atoms in the condensate and a the scattering length. We take $a = 2.93 \times 10^{-9} m$. Then we change to the lab frame where the trap moves with velocity v_0 . The ground state ψ_0 in this reference frame is $\psi_0(x) = e^{ix \frac{mv_0}{\hbar}} \bar{\psi}_0(x)$. At $t = 0$ the trap is turned off being at position x_{TRAP} and the velocity selection potentials are switched on, i.e., the time-evolution is given by the Gaussian version of the Hamiltonian of Eq. (1) plus a term V' representing the decaying nonlinear effect due to free expansion in y and z directions, $V' = 2\hbar N a \omega_{yz} |\psi(x)|^2 / (1 + \omega_{yz}^2 t^2)$. Fig. 5 shows the momentum distribution at $t = 0$ (ground state). At $t = 0.8 s$ the non-linearity has practically vanished, so the momentum distribution stays stable until the velocity selection. The filtered distributions at $t = 8 s$ for several resonance velocities obtained with different well depths are also shown.

We have in summary proposed an improvement of

Fabry-Perot cavities to select the velocity of ultra-cold atoms using a well between the partially reflecting mirrors, and have provided simple formulae to explain and describe their behaviour and the minimal velocity peak (zero) and width (non-zero) that can be achieved.

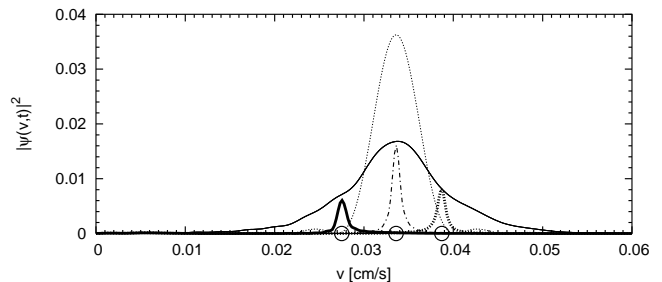


FIG. 5: $|\psi(v, t)|^2$ for $v_0 = 0.0336$ cm/s, $x_{TRAP} = -600 \mu\text{m}$; $\hat{V}_b = 300\hbar/s$, $\omega_x = 5/s$, $\omega_{yz} = 100/s$, $N = 5 \times 10^4$; $t = 0$ (dotted line); $t = 0.8s$: solid line; $t = 8s$: $\hat{V}_w = 140\hbar/s$ (thick dotted line), $\hat{V}_w = 150\hbar/s$ (dashed line), $\hat{V}_w = 160\hbar/s$ (thick solid line); the circles mark the resonance velocities v_R .

Acknowledgments

This work is supported by “Ministerio de Ciencia y Tecnología-FEDER” (BFM2003-01003), and UPV-EHU (Grant 15968/2004). AR acknowledges support of the German Academic Exchange Service (DAAD) and Ministerio de Educación y Ciencia.

-
- [1] P. Szriftgiser, D. Guéry-Odelin, M. Arndt, and J. Dalibard, *Phys. Rev. Lett.* **77**, 4 (1996).
 - [2] K. Moler, D. S. Weiss, M. Kasevich, and S. Chu, *Phys. Rev. A* **45**, 342 (1992)
 - [3] A. Aspect, E. Arimondo, R. Kaiser, N. Vansteenkiste and C. Cohen-Tannoudji, *Phys. Rev. Lett.* **61**, 826 (1998).
 - [4] M. Wilkens, E. Goldstein, B. Taylor, and P. Meystre, *Phys. Rev. A* **47**, 2366 (1993).
 - [5] L. Löffler, G. M. Meyer, and H. Walther, *Europhys. Lett.* **41**, 593 (1998).
 - [6] Z. M. Zhang, S. W. Xie, Y. L. Chen, Yu X. Xia, S. K. Zhou, *Phys. Rev. A* **60**, 3321 (1999).
 - [7] V.I. Kukulin, V.M. Krasnopol'sky, and J. Horáček, *Theory of Resonances*, (Kluwer, Dordrecht, 1989).
 - [8] D. Bohm, *Quantum Theory*, (Dover, New York, 1951).
 - [9] J.R. Angelin and W. Ketterle, *Nature* **416**, 211 (2002).
 - [10] K. Bongs and K. Sengstock, *Rep. Prog. Phys.* **67**, 907 (2004).